ISSN 1062-8738, Bulletin of the Russian Academy of Sciences. Physics, 2015, Vol. 79, No. 9, pp. 1180–1185. © Allerton Press, Inc., 2015.
Original Russian Text © A.L. Bugaev, A.A. Guda, K.A. Lomachenko, L.A. Bugaev, A.V. Soldatov, 2015, published in Izvestiya Rossiiskoi Akademii Nauk. Seriya Fizicheskaya, 2015, Vol. 79, No. 9, pp. 1329–1334.

# Pd Hydride and Carbide Studied by Means of Pd *K*-edge X-ray Absorption Near-Edge Structure Analysis

**A. L. Bugaev, A. A. Guda, K. A. Lomachenko, L. A. Bugaev, and A. V. Soldatov**

*Faculty of Physics, Southern Federal University, Rostov-on-Don, 344090 Russia*

*e-mail: abugaev@sfedu.ru*

**Abstract**—A Pd *K*-edge X-ray absorption near edge structure (XANES) analysis for palladium hydride and carbide nanoparticles is presented. It is shown that the presence of H and C atoms changes the Pd unoccupied *p*-electronic states, affecting the near-edge fine structure. Quantitative XANES analysis is performed using a multidimensional interpolation approach. Theoretical models of PdH and PdC clusters are developed using Monte Carlo methods. The proposed technique allow us to determine hydrogen concentrations in palladium nanoparticles and correctly reproduce all experimental features of XANES spectra for palladium hydride and carbide nanoparticles.

**DOI:** 10.3103/S1062873815010098

## INTRODUCTION

Palladium nanoparticles have been actively studied in recent decades [1]. Palladium nanoparticles are intensively studied with the aim of improving such important catalytic reactions as the hydrogenation of petroleum resins [2], the neutralization of hydrocarbons [3–5] and vapors of CO and $NO_x$, the hydrogenation of unsaturated hydrocarbons, the purification of terephthalic acid [6, 7], and different processes in the synthesis of fine chemical technology [8–10]. The main share of palladium consumption falls on the automotive industry. It is used in the catalysts of the exhaust system by reducing the contents of harmful impurities (such as carbon monoxide) in the exhaust of a vehicle.

As bulk samples, palladium nanoparticles are capable of absorbing hydrogen to form a hydride phase. As in bulk samples, α and β phase nanoparticles of palladium are observed, but the corresponding concentration of hydrogen depends on the size of the nanoparticles [11, 12]. The size of nanoparticles affects not only the phase diagrams, but also the kinetics of hydrogen absorption/desorption [12–15]. In small-sized nanoparticles the hydride phase is unstable [16], but different phases are observed even in nanoparticles with sizes of ~1.5 nm [11, 13, 17, 18]. Several theoretical studies have shown that the concentration of hydrogen in the near-surface layers of a nanoparticle can be higher than in its core [19-21]. The formation of palladium hydride changes the catalytic activity of nanoparticles [22-25]. It is believed that hydrogen is more energetically active in the inner part of a nanoparticle, and it is able to hydrogenate reactants upon emerging on the surface of nanoparticles [13, 26].

In contrast to the hydride phase, the formation of the palladium carbide phase remains poorly studied. There are indications that palladium–carbon atomic bonds are quite strong, and it is impossible to get rid of them even after prolonged heat treatment [27, 28].

In this work, we analyze the fine structure of X-ray absorption spectra near the absorption edge (XANES) for the *K*-edge of palladium. This method is sensitive to changes in unoccupied states with *p*-symmetry with respect to palladium atoms. Quantitative analysis of the near-threshold regions of absorption spectra allows to extract information on the concentration of hydrogen and carbon atoms inside palladium nanoparticles, and on their location.

## EXPERIMENTAL

Experimental X-ray absorption spectra of palladium hydride nanoparticles were registered on the Swiss–Norwegian BM01b line at the European Synchrotron Radiation Center (ESRF) in Grenoble, France. The spectra were measured in the passage mode, using ionization chambers. At the same time, we measured the X-ray absorption spectrum of a standard sample of palladium foil, allowing us to control any possible energy shift. The sample was placed in a glass capillary with a diameter of 1 mm. During the experiment, the temperature and pressure of hydrogen in the capillary was varied, allowing us to obtain different degrees of hydrogen saturation for palladium nanoparticles. A schematic representation of the measurement procedure is shown in Figure 1. The diagram shows the final compartment of the BM01b synchrotron line, controlled by a PC. Capillary *2* with the sample was placed in holder *1* of the spectrometer. The sample was palladium nanoparticles on the substrates of aluminum oxide. Gas heater *3* was placed beneath capillary *2*, and capillary pipe *4* was connected to gas

unit *5*. For simplicity, the capillary in the scheme is connected to only one side, though in reality it was connected to both sides. The outputs of the gas system were connected to vessel *6* filled with hydrogen. A beam of monochromatic X-ray radiation was emitted from X-ray source *7* in the direction of the sample. Input and output detectors (ionization chambers *8* and *9*) are arranged on the path of the X-ray beam in front of and behind the sample and correspond to the passage scheme. Input and output detectors *8* and *9* measure the X-ray intensity before and after passing through the capillary and the sample. When switching from the measuring mode of the X-ray absorption spectrum to the diffraction mode, a two-dimensional diffraction detector was placed in front of output detector *9*. Temperature *T* was controlled by gas heater *3*. Gas system *5* allowed us to pump hydrogen into and out of the capillary with sample *2*. To obtain spectra of X-ray absorption and diffraction patterns, the temperature and pressure are fixed as is required in the experiment. The intensities of X-ray radiation are then automatically measured using detectors at inlet *8* and outlet *9*. A more detailed description of the experimental setup and measurement procedure can be found in [29]. X-ray absorption spectra for palladium carbide nanoparticles were obtained by our colleagues [28] on the X10DA (SuperXAS) line of the SLS synchrotron source (Villigen, Switzerland). Measurements were made in the passage mode. The experimental EXAFS spectra were processed using the IFEFIT software [30]. Processing included background subtraction, normalization, energy calibration, Fourier transformation, and fitting using the phases and amplitudes calculated with the FEFF6 code [31].

To determine the interatomic distances, fitting was performed in real space in the range of 1.5 to 3.0 Å, using weighted $k^2$ spectra in the range of 5 to 12 Å$^{-1}$. The interatomic distances ($R_{Pd-Pd}$), the Debye–Waller factor ($\sigma^2$), the energy shift ($\Delta E_0$), and coordination number were used as the fitting parameters in approximating the spectra obtained upon hydrogen absorption. In analyzing the palladium foil spectra, a value of 0.82 was obtained for factor $S_0^2$ and used for all nanoparticles. The parameters $\Delta E_0$ and $N$ were common to all of the fitted spectra. This approach allowed us to perform simultaneous fitting of a number of spectra and to reduce the number of variable parameters.

The Debye correlation model was used to reduce the number of independent parameters, allowing us to describe the temperature dependence of the Debye–Waller parameter $\sigma^2(T)$ [32] for the fitting of the desorption spectra obtained by varying temperature.

## RESULTS AND DISCUSSION

Palladium nanoparticles were synthesized via wet impregnation [11, 27, 28]. The gamma phase of aluminum oxide $Al_2O_3$ and silica $SiO_2$ with pore volumes of 180 and 300 m$^2$/g were used as the porous substrate. In addition, a solution of $Pd(NH_3)_4(NO_3)_2$ was used as the precursor. The samples were annealed at varying parameters of temperature and annealing time and then cleansed of surface oxidation in a hydrogen stream. A sample for detailed analysis was synthesized on a substrate of alumina. Annealing was done at 250°C for 5 hours.

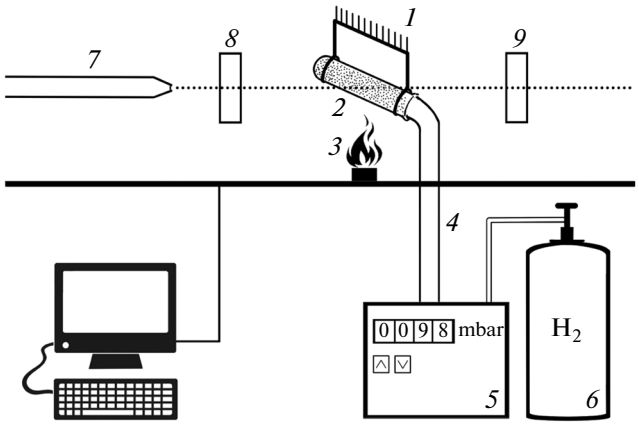


**Fig. 1.** Experimental setup for measuring X-ray absorption spectra for the *K*-edge of palladium in palladium nanoparticles. The notation is explained in the text.

The oxygen was purified in an atmosphere of pure hydrogen at a temperature of 250°C for 5 hours. Powder-like samples were black in color. Preliminary analysis of the samples was performed by means of transmission electron microscopy and X-ray diffraction. We used a JEM-2010F FasTEMm FEI microscope manufactured by JEOL.

To obtain high quality images of palladium nanoparticles on an aluminum substrate, the electron microscope was operated in the *Z*-contrast mode at a voltage of 200 kV. Measuremnets were made with the electron microscope both before and after the nanoparticles were saturated with hydrogen. A series of transmission electron microscopy images containing ~100 different nanoparticles was analyzed to estimate the average particle size. The resulting average particle size was 9.5 nm. Most of the particles were nonspherical, due possibly to their partial agglomeration. The absorption and desorption of hydrogen had no effect on the shape or size of the particles.

An alternative analysis of the average crystallite size was performed via XRD. The distribution of crystallite size was obtained by analyzing the broadening of the peak corresponding to the (111) reflections of palladium. This analysis was performed using the L&TGSD software package [33], in which the FW 1/5/4/5 M method is implemented. It is based on measuring the peak width at heights of 1/5 and 4/5 of entire peak height. The resulting average crystallite size was 5.2 nm, which is smaller than the average size

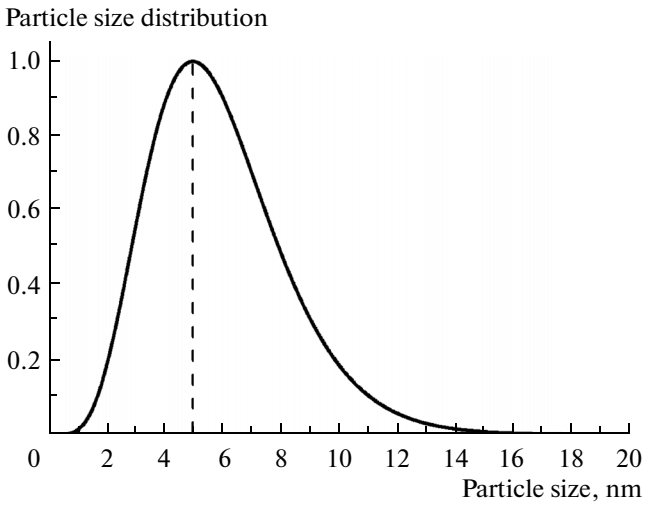


**Fig. 2.** Crystallite size distribution in the region of coherent scattering, obtained using data from X-ray diffraction.

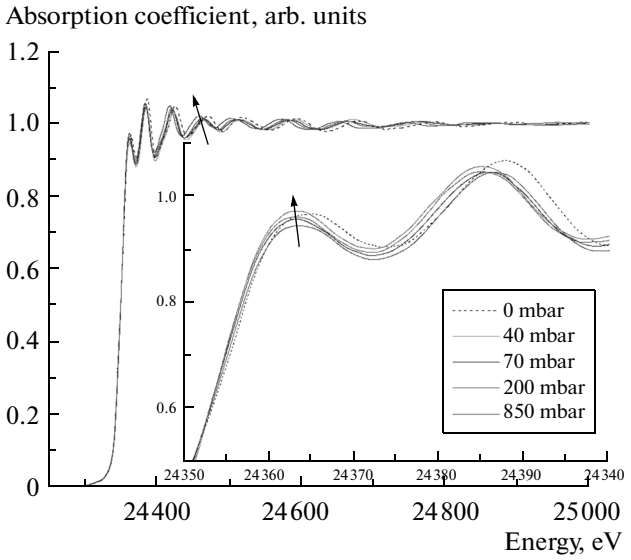


**Fig. 3.** Experimental X-ray absorption spectra behind the *K*-edge for palladium nanoparticles at different hydrogen pressure. The insert shows the near-threshold region of the spectra. The arrows indicate the direction corresponding to the increase in the concentration of hydrogen. The dotted line represents the spectrum of pure nanoparticles.

of nanoparticles obtained according to transmission electron microscopy. This indicates that the region of coherent scattering of nanoparticles was less than was visually determined by electron microscopy. This effect could also be due to nanoparticle agglomeration. The size distribution of the crystallites is shown in Fig. 2.

The experimental X-ray absorption spectra are shown in Fig. 3. In saturating the nanoparticles with hydrogen, the maxima of the spectra shift to lower energies due to the increasing Pd–Pd interatomic distance. According to EXAFS analysis, the interatomic distances for pure nanoparticles were $2.74 \pm 0.01$ Å. It is worth noting that an absolute error on the order of 0.01 Å is usual for EXAFS analysis [34, 35], and relative changes $\Delta R$ in the interatomic distances can be determined with much greater accuracy [36, 37]. More than 15 different interatomic distances can thus be successfully determined in the range of 2.74 to 2.81 Å. After isobaric desorption, the interatomic distances fell to 2.75A, testifying to the reversible nature of the hydride phase.

Along with the changes in the interatomic distances, a 0.001 Å$^2$ increase in the Debye-Waller factor was observed for the hydride phase. Such an increase (at constant temperature) suggests that the hydride phase is more disordered. On the one hand, this disorder could be chaotic; on the other hand, it could be due to the formation of structures with saturated hydrogen shells and hydrogen-depleted metal cores. Such model structures have been obtained in some theoretical studies [19-21]. In the latter case, we can reduce the Debye–Waller factor with a series of adjustments to the fitting procedure. This scheme was demonstrated for pure palladium nanoparticles [38].

The theoretical XANES spectra were calculated with full multiple scattering using the Hedin–Lundquist exchange-correlation potential implemented in the FEFF8.4 code [31, 40]. Test calculations for atomic clusters with radii from 3 Å to 10 Å showed that the spectra converge at a cluster atomic radius of 7.5 Å. XANES fitting of experimental data was performed via multivariate interpolation [41], implemented in the Fitit 3.01 code [42].

As is known from the literature, X-ray absorption spectra for the $L_3$-edge of Pd are very sensitive to the presence of hydrogen, due to changes in the electron states with *d*-symmetry relative to Pd atoms (during hydrid phase formation). Such XANES spectra are usually regarded as the only source of direct information on the presence of hydrogen atoms in the structure. However, measuring the absorption spectra for light edges is a more difficult experimental task, especially when measurements in situ under hydrogen pressure are required. This is why we showed that the spectra of the *K*-edge of palladium, which reflect the change in the electronic states with *p*-symmetry with respect to palladium atoms, are also sensitive to the formation of the hydride phase [43]. Theoretical calculations indicate that the increase in the intensity of the first edge maximum in the absorption spectra is associated with the mixing of unoccupied *d*-electron states of palladium and the *s*- and *p*- unoccupied states of hydrogen. We showed in [29] that the relative intensity of first edge maxima can be used for rapid qualitative analysis of palladium hydride phase formation.

Geometrical models for calculating theoretical absorption spectra were constructed using Monte

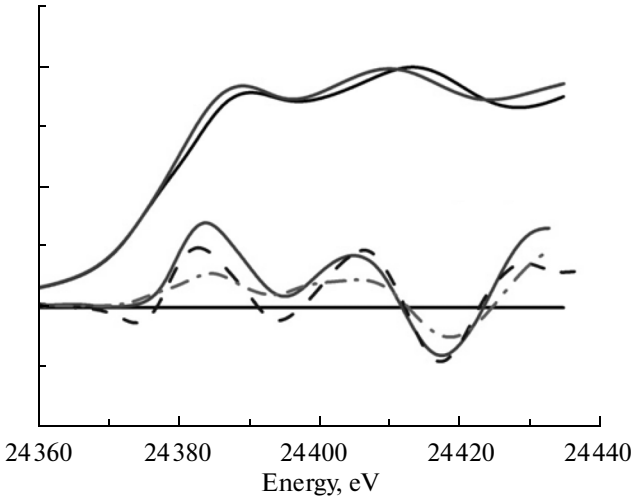


**Fig. 4.** Fitting of the experimental difference spectra. Experimental XANES spectra (top) and difference spectra (bottom) for pure and hydrogenated nanoparticles are shown by solid lines. The dashed curve shows the difference spectrum calculated with allowance for hydrogen atoms. The dashed-and-dotted curve shows the difference spectrum calculated with a formal increase in the interatomic distances Pd–Pd to values corresponding the palladium hydride. The ordinates are arbitrary values.

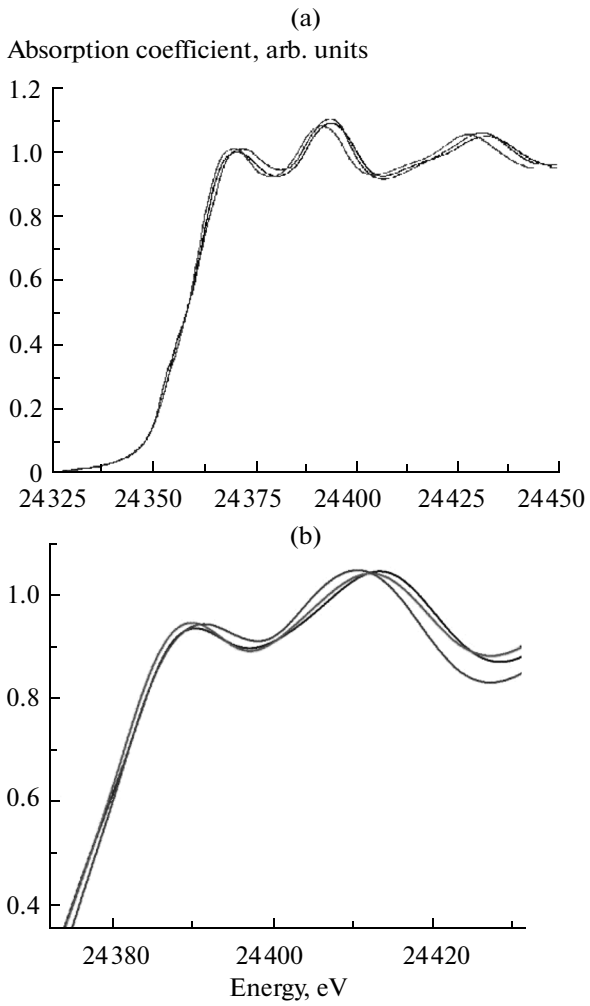


**Fig. 5.** Changes in (a) experimental and (b) theoretical XANES absorption spectra behind the *K*-edge in the formation of palladium hydride and carbide phase in nanoparticles of palladium.

Carlo methods to allow for the statistical distribution of hydrogen and carbon atoms. Preliminary analysis showed that when averaging two series consisting of more than 200 spectra, the difference between the averaged spectra is negligible. Around 1000 different geometric configurations were thus generated for each predetermined concentration, calculated on a supercomputer, and then averaged. To monitor the accuracy of the geometric models, the distribution of the number of hydrogen atoms was tested around the central (absorbing) palladium atom. In all cases, this distribution proved to be close to normal. The spectra calculated in this manner repeat all of the experimental characteristics, including the increase in the relative intensity of $I_A/I_B$, the changes in the pre-edge region, and the shift of the first peak toward lower energies (Fig. 4).

To obtain hydrogen concentrations, the difference spectra for each experimental spectrum were fitted by means of multivariate interpolation using the Fitit 3.01 code [42]. Theoretical spectra for pure palladium and hydrides of $PdH_{0.3}$ and $PdH_{0.5}$ with different interatomic distances (2.75 Å, 2.78 Å, and 2.81 Å) were used as nodes for constructing the interpolation polynomial. The interpolation polynomial of the second order relative to the interatomic distances was constructed in the form $r + x + r^2 + x^2 + rx$, where parameters $r$ and $x$ correspond to interatomic distance and hydrogen concentration. To verify the results, fitting was performed for both difference spectra and the original spectrum. It led to identical results. The resulting concentration values were consistent with those obtained using such alternative techniques as thermogravimetric analysis [44] and plasmon resonance [12]. The absorption spectrum of palladium carbide nanoparticles was modeled in a similar fashion. The simulation results are shown in Fig. 5.

## CONCLUSIONS

We have presented a scheme for analyzing the hydride and carbide phase in palladium nanoparticles, based on X-ray absorption spectra behind the *K*-edge of palladium. It was shown that a correct description of the experimental spectra requires direct consideration of the carbon and hydrogen atoms in the theoret-

ical model, and of their statistical distribution. The use of multivariate interpolation reduces the number of calculated spectra. Our scheme allows us to obtain quantitative values for the concentrations of hydrogen and carbon in palladium nanoparticles. A similar approach can be extended to a number of objects containing impurities and defects of different types in unknown concentrations.

## ACKNOWLEDGMENTS

This work was performed under RF Presidential Grant No. MK-3206.2014.2 for the Support of Young Scientists and RF Government Grant No. 14.Y26.31.0001 for the State Support of Research Conducted under the Supervision of Leading Scientists.

## REFERENCES

1. Tungler, A., Tarnai, T., Hegedus, L., Fodor, K., and Máthé, T., *Platinum Met. Rev.*, 1998, vol. 42, no. 3, p. 108.
2. Yu, L.J., Jiang, D.H., Xu, J., Ma, L., and Li, X.N., *China Pet. Process. Petrochem. Technol.*, 2012, vol. 14, no. 3, p. 83.
3. Lampert, J.K., Kazi, M.S., and Farrauto, R.J., *Appl. Catal., B*, 1997, vol. 14, nos. 3–4, p. 211.
4. Gelin, P. and Primet, M., *Appl. Catal., B*, 2002, vol. 39, no. 1, p. 1.
5. Liotta, L.F., *Appl. Catal., B*, 2010, vol. 100, nos. 3–4, p. 403.
6. Pernicone, N., Cerboni, M., Prelazzi, G., Pinna, F., and Fagherazzi, G., *Catal. Today,* 1998, vol. 44, nos. 1–4, p. 129.
7. Pellegrini, R., Agostini, G., Groppo, E., Piovano, A., Leofanti, G., and Lamberti, C., *J. Catal.*, 2011, vol. 280, no. 2, p. 150.
8. Blaser, H.U., Indolese, A., Schnyder, A., Steiner, H., and Studer, M., *J. Mol. Catal. A: Chem.*, 2001, vol. 173, nos. 1–2, p. 3.
9. Garrett, C.E. and Prasad, K., *Adv. Synth. Catal.*, 2004, vol. 346, no. 8, p. 889.
10. Torborg, C. and Beller, M., *Adv. Synth. Catal.*, 2009, vol. 351, no. 18, p. 3027.
11. Tew, M.W., Miller, J.T., and van Bokhoven, J.A., *J. Phys. Chem. C*, 2009, vol. 113, no. 34, p. 15140.
12. Langhammer, C., Larsson, E.M., Kasemo, B., and Zoric, I., *Nano Lett.*, 2010, vol. 10, no. 9, p. 3529.
13. Ingham, B., Toney, M.F., Hendy, S.C., Cox, T., Fong, D.D., Eastman, J.A., Fuoss, P.H., Stevens, K.J., Lassesson, A., and Brown, S., *Phys. Rev. B*, 2008, vol. 78, no. 24, p. 245408.
14. Yamauchi, M., Ikeda, R., Kitagawa, H., and Takata, M., *J. Phys. Chem. C,* 2008, vol. 112, no. 9, p. 3294.
15. Agostini, G., Lamberti, C., Pellegrini, R., Leofanti, G., Giannici, F., Longo, A., and Groppo, E., *ACS Catal.*, 2014, vol. 4, no. 1, p. 187.
16. Bérubé, V., Radtke, G., Dresselhaus, M., and Chen, G., *Int. J. Energy Res.*, 2007, vol. 31, nos. 6–7, p. 637.
17. Jobic, H. and Renouprez, A., *J. Less Common Met.*, 1987, vol. 129, p. 311.
18. Narehood, D., Kishore, S., Goto, H., Adair, J., Nelson, J., Gutierrez, H., and Eklund, P., *Int. J. Hydrogen Energy*, 2009, vol. 34, no. 2, p. 952.
19. Langhammer, C., Zhdanov, V.P., Zorić, I., and Kasemo, B., *Chem. Phys. Lett.*, 2010, vol. 488, no. 1, p. 62.
20. Langhammer, C., Zhdanov, V.P., Zorić, I., and Kasemo, B., *Phys. Rev. Lett.*, 2010, vol. 104, no. 13, p. 135502.
21. Zhdanov, V.P. and Kasemo, B., *Chem. Phys. Lett.*, 2008, vol. 460, no. 1, p. 158.
22. Johnson, A., Daley, S., Utz, A., and Ceyer, S., *Science*, 1992, vol. 257, no. 5067, p. 223.
23. Haug, K., Buergi, T., Trautman, T., and Ceyer, S., *J. Am. Chem. Soc.*, 1998, vol. 120, no. 34, p. 8885.
24. Teschner, D., Borsodi, J., Wootsch, A., Revay, Z., Havecker, M., Knop-Gericke, A., Jackson, S.D., and Schlogl, R., *Science*, 2008, vol. 320, no. 5872, p. 86.
25. Chase, Z.A., Fulton, J.L., Camaioni, D.M., Mei, D., Balasubramanian, M., Pham, V.-T., Zhao, C., Weber, R.S., Wang, Y., and Lercher, J.A., *J. Phys. Chem. C*, 2013, vol. 117, no. 34, p. 17603.
26. Morkel, M., Rupprechter, G., and Freund, H.-J., *Surf. Sci.*, 2005, vol. 588, no. 1, p. L209.
27. Tew, M.W., Janousch, M., Huthwelker, T., and van Bokhoven, J.A., *J. Catal.*, 2011, vol. 283, no. 1, p. 45.
28. Tew, M.W., Nachtegaal, M., Janousch, M., Huthwelker, T., and van Bokhoven, J.A., *Phys. Chem. Chem. Phys.,* 2012, vol. 14, no. 16, p. 5761.
29. Bugaev, A.L., Guda, A.A., Lomachenko, K.A., Srabionyan, V.V., Bugaev, L.A., Soldatov, A.V., Lamberti, C., Dmitriev, V.P., and van Bokhoven, J.A., *J. Phys. Chem. C*, 2014, vol. 118, no. 19, p. 10416.
30. Ravel, B. and Newville, M., *J. Synchrotron Radiat.*, 2005, vol. 12, no. 4, p. 537.
31. Rehr, J.J. and Albers, R.C., *Rev. Mod. Phys.*, 2000, vol. 72, no. 3, p. 621.
32. Beni, G. and Platzman, P., *Phys. Rev. B*, 1976, vol. 14, no. 4, p. 1514.
33. Leontyev, I., Guterman, V., Pakhomova, E., Timoshenko, P., Guterman, A., Zakharchenko, I., Petin, G., and Dkhil, B., *J. Alloys Compd.*, 2010, vol. 500, no. 2, p. 241.
34. *X-Ray Absorption: Principles, Applications, Techniques of EXAFS, SEXAFS and XANES*, Koningsberger, D.C. and Prins, R., Eds., John Wiley and Sons, 1987.
35. Bordiga, S., Groppo, E., Agostini, G., van bokhoven, J.A., and Lamberti, C., *Chem. Rev.*, 2013, vol. 113, no. 3, p. 1736.
36. Pettifer, R.F., Mathon, O., Pascarelli, S., Cooke, M.D., and Gibbs, M.R., *Nature,* 2005, vol. 435, no. 7038, p. 78.

37. Romanato, F., de Salvador, D., Berti, M., Drigo, A., Natali, M., Tormen, M., Rossetto, G., Pascarelli, S., Boscherini, F., Lamberti, C., and Mobilio, S., *Phys. Rev. B,* 1998, vol. 57, no. 23, p. 14619.

38. Srabionyan, V.V., Bugaev, A.L., Pryadchenko, V.V., Avakyan, L.A., van Bokhoven, J.A., and Bugaev, L.A., *J. Phys. Chem. Solids*, 2014, vol. 75, no. 4, p. 470.

39. Hedin, L. and Lundqvist, B.I., *J. Phys. C: Solid State Phys.*, 1971, vol. 4, no. 14, p. 2064.

40. Rehr, J.J. and Ankudinov, A.L., *Coord. Chem. Rev.,* 2005, vol. 249, nos. 1–2, p. 131.

41. Smolentsev, G. and Soldatov, A., *J. Synchrotron Radiat.*, 2005, vol. 13, no. 1, p. 19.

42. Smolentsev, G. and Soldatov, A.V., *Comput. Mater. Sci.*, 2007, vol. 39, no. 3, p. 569.

43. Bugaev, A.L., Srabionyan, V.V., Soldatov, A.V., Bugaev, L.A., and van Bokhoven, J.A., *J. Phys.: Conf. Ser.*, 2013, vol. 430, p. 012028.

44. Kishore, S., Nelson, J., Adair, J., and Eklund, P., *J. Alloys Compd.*, 2005, vol. 389, no. 1, p. 234.

*Translated by G. Dedkov*